Biophysical Journal
Article

Biophysical Society

DNA Local-Flexibility-Dependent Assembly of Phase-Separated Liquid Droplets

Anisha Shakya[1] and John T. King[1,*]
[1]Institute for Basic Science, Center for Soft and Living Matter, Ulsan, Republic of Korea

ABSTRACT Phase separation of intracellular components has been recently realized as a mechanism by which cells achieve membraneless organization. Here, we study the associative liquid-liquid phase separation (LLPS) of DNA upon complexation with cationic polypeptides. Comparing the phase behavior of different single-stranded DNA as well as double-stranded DNA (dsDNA) sequences that differ in persistence lengths, we find that DNA local flexibility, not simply charge density, determines the LLPS. Furthermore, in a nucleotide- and DNA-dependent manner, free nucleotide triphosphates promote LLPS of polypeptide-dsDNA complexes that are otherwise prone to precipitation. Under these conditions, dsDNA undergoes a secondary phase separation forming liquid-crystalline subcompartments inside the droplets. These results point toward a role of local DNA flexibility, encoded in the sequence, in the regulation and selectivity of multicomponent LLPS in membraneless intracellular organization.

INTRODUCTION

Liquid-liquid phase separation (LLPS) has emerged as an important phenomenon in biology, involved in processes ranging from the formation of membraneless bodies like ribonucleoprotein granules and nucleolus to domain organization in heterochromatin (1–6). This phenomenon draws close analogy to complex coacervation, which refers to the formation of a distinct liquid-like phase when oppositely charged polymers (polyelectrolytes) are mixed in a single solvent (7). The proteins that undergo LLPS typically contain intrinsically disordered regions rich in charged amino acids (1–4). For some proteins, LLPS is enhanced in the presence of nucleic acids (NAs), with the phase diagram and physical properties of resulting droplets being dependent on the type of NA (8). For such multicomponent LLPS, it is not clear how the sequence of individual components plays a role. Emerging studies on protein LLPS suggest that the pattern of charges in the protein sequence dictates LLPS rather than simply the overall charge (9). The role of NA sequence on the other hand is yet to be explored.

Two interactions are key to the NA structure: electrostatic repulsions (primarily due to the backbone phosphates) and base stacking interactions (10–12). These interactions, the former being highly salt-dependent and the latter being sequence-dependent, determine the flexibility of NA (12,13). Here, we employ multicomponent systems based on DNA and a cationic homopolypeptide, poly-L-lysine (PLL) (Fig. 1 *a*), to study the role of DNA flexibility in determining LLPS. Complex NA sequences are prone to forming secondary and tertiary structures, making it difficult to dissect the role of intrinsic flexibility owing to polymer properties. Therefore, we employ homopolymeric and simple DNA sequences as model systems. Three key findings are reported: 1) basepairing interaction in DNA is unfavorable for LLPS; 2) DNA local flexibility, encoded by the DNA sequence, not simply the overall charge density, determines the phase behavior; 3) the presence of free nucleotide triphosphates promotes LLPS in both a nucleotide- and DNA-specific manner. Interestingly, in the case of double-stranded DNA (dsDNA), a secondary phase separation occurs, giving rise to liquid-crystalline dsDNA subcompartments within the droplets.

MATERIALS AND METHODS

Materials

PLL (MW 30–70 kDa), nucleotide triphosphates (NTPs) (sodium salt), Tris-EDTA buffer (10 mM Tris-HCl, 1 mM EDTA, (pH 7.4)), and sodium chloride were obtained from Sigma (St. Louis, MO). All oligonucleotides (labeled as well as unlabeled) were obtained from Integrated DNA Technologies (Skokie, Illinois) in dry form and subsequently dissolved in Tris-EDTA buffer. Rhodamine-6G (R6G)-labeled ATP (ATP-R6G) was obtained from Perkin Elmer (Waltham, MA). AlexaFluor488 (AF488)-labeled

Submitted May 14, 2018, and accepted for publication September 7, 2018.
*Correspondence: jtking@unist.ac.kr
Editor: Gijs Wuite.
https://doi.org/10.1016/j.bpj.2018.09.022

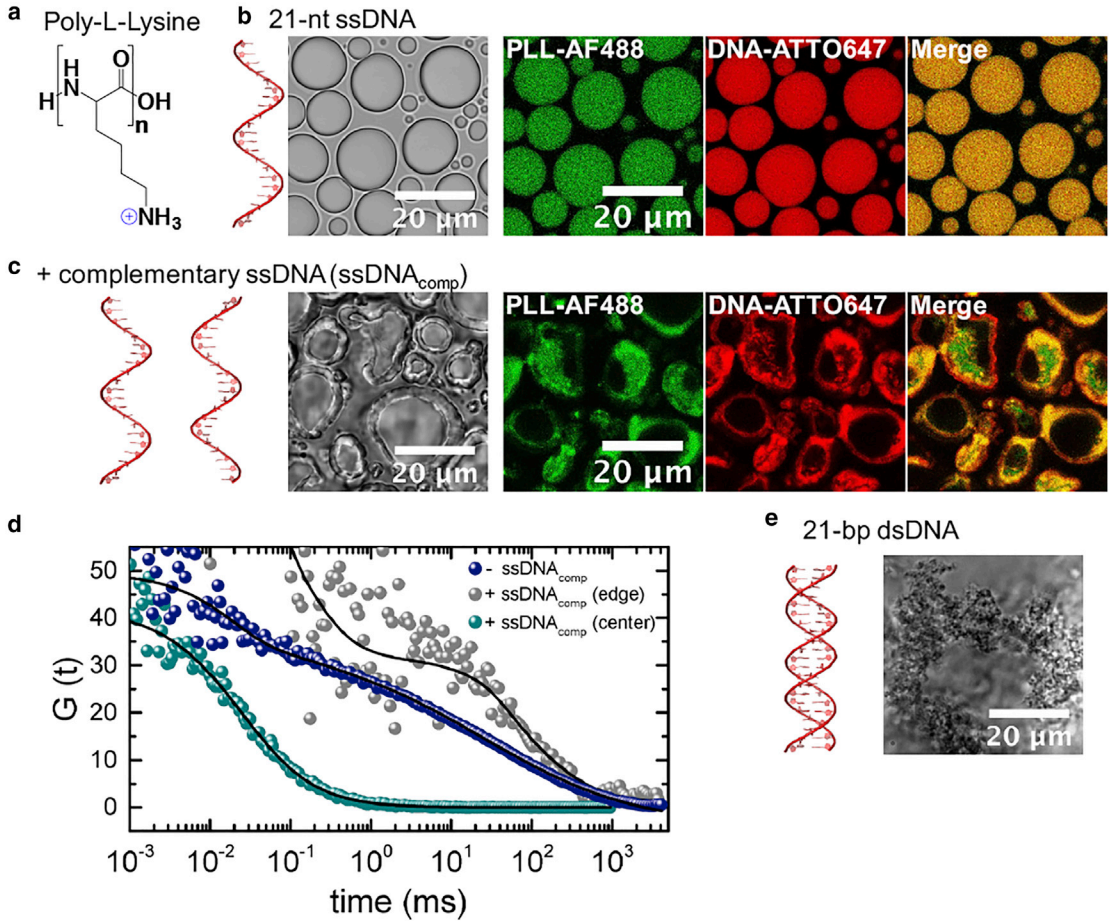

FIGURE 1 DNA rigidity due to basepairing is unfavorable for LLPS. (*a*) The chemical structure of PLL. (*b*) Phase-separated droplets of PLL and a random sequence 21-nt ssDNA; [NaCl] = 150 mM, N/P ~1, room temperature. Confocal fluorescence images show homogenous partitioning of both PLL and ssDNA. (*c*) Coarsened and hollow structures resulting after the addition of a 1:1 equivalent of complementary ssDNA (ssDNA$_{comp}$) to preformed PLL-ssDNA droplets shown in (*b*); resulting N/P ~0.4. The distribution of PLL and DNA is heterogeneous, with both polymers preferentially partitioned close to the droplet/solution interface. (*d*) FCS autocorrelation curves are measured for labeled PLL before ($\tau_{transit}$ = 28 ms) and after ($\tau_{transit}$ = 120 ms at the *edges* and $\tau_{transit}$ = 0.029 ms in the interior of the *hollow structures*) the addition of ssDNA$_{comp}$. The dynamics are significantly reduced at the edges, whereas the interior is near water like. (*e*) A bright-field image of precipitates of PLL-dsDNA complexes under the same conditions of salt, temperature, and N/P as in (*b*).

uridine triphosphate (UTP) (UTP-AF488) and YOYO-1 were obtained from ThermoScientific (Waltham, MA).

All ssDNAs were annealed by heating at 95°C for 5 min and cooling in ice for at least 1 h. The DNA was then exchanged into the desired buffer. All dsDNAs were annealed using a thermocycler; 2–4 mM solutions in Tris-EDTA buffer were heated at 95°C for 5 min, slowly cooled over at least 1 h at a rate of 1°C/min below their respective melting temperatures and held at 4°C before exchanging into the desired buffer.

Sample preparation

Eight-well 1.0 borosilicate chambered glass slides (Nunc Lab Tek; ThermoScientific) were cleaned with RNase Zap (Ambion; ThermoScientific), ethanol, and nuclease-free water and were ultraviolet treated overnight. The glass surface was passivated using 3.5% bovine serum albumin solution (Sigma) for 15 min at room temperature, rinsed three times with nuclease-free water, and dried. PLL-DNA mixtures were then added to the bovine serum albumin passivated glass chambers, sealed with biocompatible glue (JPK Instruments, Berlin, Germany), and imaged under a bright-field microscope, typically after 2 h of incubation at room temperature.

The positive/negative charge ratio (or lysine/phosphate ratio (N/P)) of all the mixtures (unless specified) was estimated to be ~1, assuming 240 monomer units (average molecular weight/monomer molecular weight) per mole of PLL (i.e., 240 positive charges per PLL) and one negative charge per phosphate group in the nucleotide. For free nucleotides, 4 mol of charge per mole of nucleotide was assumed.

Comparison of phase separation of 21-nt ssDNA versus 21-bp dsDNA

A 21-nucleotide (nt) ssDNA random sequence, 5′-CTTACGCTGAGTA CTTCGATT-3′, was used. 0.2 mM 21-nt ssDNA was prepared in Tris-EDTA buffer with no added salt. 16 μM PLL was prepared in Tris-EDTA buffer with 300 mM of NaCl and added to the oligonucleotide solution in a 1:1 volume ratio (final [NaCl] = 150 mM). For confocal imaging, the samples contained 1 nM AF488-labeled PLL (PLL-AF488) (~5 AF488 per PLL) and 5 nM ATTO647-labeled 21-nt ssDNA (DNA-ATTO647). An equimolar amount of complementary strand was added to preformed PLL-ssDNA droplets to observe the effect of basepairing. As a control experiment, an equimolar amount of noncomplementary strand (same ssDNA) was added to preformed PLL-ssDNA droplets.

Preannealed 21-basepair (bp) dsDNA of the same sequence was also mixed with PLL at a final NaCl concentration of 150 mM and N/P ~1, which resulted in precipitation. To test whether the 21-bp dsDNA form liquid-like phases at high salt, phase separation experiments were carried out at 730 and 830 mM NaCl.

Sequence effects on phase separation

The following oligonucleotide sequences were used in these experiments: 22-nt polyadenine (poly(A)), 22-nt polythymidine (poly(T)), 22-nt poly(C), palindromic 22-bp poly(GC) (5′-GGGCCGGCCGGCCGGCCGGCCC-3′), and palindromic 22-bp poly(AT) (AAATTAATTAATTAATTAATTT-3′).

2 mM PLL stock and 2 mM DNA stock were diluted in Tris-EDTA buffer such that the final N/P was ~1 after mixing PLL and DNA at a 1:1 volume ratio. PLL was prepared in 2× NaCl buffer, and DNA was prepared in no-salt buffer to reach the desired salt concentration after mixing. The order of mixing was always PLL solution into DNA solution.

Role of free nucleotides in phase separation of dsDNA

0.1 mM 22-bp dsDNA stock, 100 mM NTP stock, and 2 mM PLL stock were mixed such that the final N/P was ~1 (~2 mM positive charge from PLL, 0.7 mM negative charge from dsDNA, and 1.4 mM negative charge from NTP in the final volume). The final NaCl concentration was 150 mM. In all cases, the mixing order was DNA to NTP solution (1:1 volume ratio) followed by PLL to DNA-NTP solution (1:1 volume ratio). For confocal fluorescence and fluorescence correlation spectroscopy (FCS) experiments, ATP-R6G or UTP-AF488 was added at a final concentration of 5 nM. For UTP, higher concentration was required for forming droplets comparable to that of PLL-dsDNA-ATP. N/P of ~0.2 (UTP charge = 7 mM) was used to form UTP-containing droplets.

Partitioning of dsDNA in phase-separated droplets

dsDNA intercalating dye YOYO-1 was used to label poly(GC) and poly(AT) (labeling density of 1 YOYO-1 per 42 bp) to observe partitioning of the dsDNA into the droplets. FCCS experiments were performed using nanomolar amounts of 22-bp dsDNA labeled at the 5′ ends of the complementary strands (poly(A)-ATTO647 and poly(T)-AF488) as the probe. The dual-color dsDNA was mixed with unlabeled poly(AT) to form PLL-poly(AT)-UTP droplets at N/P of ~0.2 and 150 mM NaCl. Control experiments were performed by adding nanomolar concentrations of unannealed (single-stranded) poly(A)-ATTO647 and poly(T)-AF488 to unlabeled poly(AT) to form PLL-poly(AT)-UTP droplets.

Bright-field imaging

Bright-field images were obtained using a Leica DMI6000 B microscope (Leica Microsystems, Wetzlar, Germany) using 100× oil objective and Grasshopper3 camera (Point Grey, Richmond, BC, Canada) with 2048 × 2048 resolution and pixel size of 5.5 μM. Images were processed to adjust brightness, contrast, and image size using the ImageJ software (14).

Confocal fluorescence imaging

An unmodified commercial stimulated emission depletion microscopy setup (SP8x; Leica Microsystems) was used (100× oil objective; 1.45 NA). Excitations (5–50% excitation power at 70% master power) at either 488, 514, or 633 nm with respective detection band pass of 500–550, 555–595, or 647–703 nm were used depending on the chromophore label (AF488 and YOYO-1, R6G, or ATTO647).

FCS

FCS measurements were carried out on the same Leica instrument. A pulsed white-light laser (WLL) (NKT Photonics, Birkerød, Denmark) operating at 40 MHz (master power of 70%) was used as the excitation source in all experiments. The output power was further reduced to 10% of the master power for FCS experiments. For AF488 labels, the WLL output was filtered to 488 nm for excitation. The fluorescence signal was passed through a 500–550 nm band-pass filter. For all experiments, the fluorescence signal was passed through a confocal pinhole (set to 1 Airy unit) and detected with a single-photon-counting avalanche photodiode (Micron Photon Devices, Bolzano, Italy; PicoQuant, Berlin, Germany) and recorded with a time-correlated single-photon-counting detection unit (Picoharp 300; PicoQuant). SymPhoTime software (PicoQuant) was used to time gate the data and compute FCS autocorrelation functions. The FCS autocorrelation curves were fitted with the triplet extended model in the SymPhoTime software to obtain diffusion parameters.

FCCS experiments were performed on the same Leica instrument. The WLL output was filtered to 488 and 633 nm for simultaneous excitation of AF488 and ATTO647, respectively. The fluorescence signal was passed through a confocal pinhole (set to 1 Airy unit) and was separated with a 620 nm dichroic beam splitter. The short-pass signal was passed through a 500–550 nm band-pass filter, whereas the long-pass signal was passed through a 647–703 nm band-pass filter. Two single-photon-counting avalanche photodiodes connected to a time-correlated single-photon-counting unit were used for detection. SymPhoTime software was used to time gate the data and compute the autocorrelation and crosscorrelation functions.

Role of temperature in droplet formation

Required volumes of PLL and poly(C) were prepared in 1:1 volume ratio to obtain the final N/P of ~1 and NaCl concentration of 150 mM. Both solutions were preheated to 95°C for 5 min, mixed immediately, and imaged under bright field. Droplets, instead of precipitates, were observed under the microscope under these conditions.

Cross-polarization imaging

Samples were imaged using a Leica DMI6000 B inverted microscope in transmission between crossed polarizers (depolarized transmission optical microscopy). Images were processed to adjust brightness, contrast, and image size using the ImageJ software. Background subtraction in ImageJ software (14) was used for images of PLL-dsDNA-NTP droplets to contrast the birefringent domains versus the isotropic phase.

RESULTS AND DISCUSSION

Role of DNA basepairing in LLPS

We first tested how the DNA basepairing affects LLPS. DNA flexibility is typically characterized by the persistence length, defined as the length scale beyond which a polymer is strongly bent because of thermal fluctuations (15,16). For dsDNA under physiological ionic conditions, the persistence length is ~50 nm (~150 bp), which is

much higher than its chain width (~2 nm). Therefore, below 50 nm dsDNA is considered a rigid rod (10–13,17). ssDNA, on the other hand, has a persistence length on the same order of its chain width (~1 nm) and thus is considered a flexible polymer (10–12,17). Upon mixing with PLL at 150 mM NaCl, PLL lysine to DNA phosphate ratio (N/P ~1), and room temperature, phase-separated droplets containing both PLL and ssDNA are formed (Fig. 1 *b*; Fig. S1). Upon adding complementary ssDNA ($ssDNA_{comp}$) the PLL-ssDNA droplets coarsen (Fig. 1 *c*). Under these conditions, partial basepairing between the complementary strands is expected. In a control experiment, an equimolar amount of noncomplementary ssDNA (same ssDNA) was added. In this case, no coarsening of the droplets is observed (Fig. S2). This indicates that the coarsening arises because of basepairing between the complementary DNA strands. Both PLL and DNA show preferential partitioning close to the droplet/solution interface, giving the droplets a hollow vesicle-like appearance (Fig. 1 *c*; Fig. S3). The interior of the droplets is near water like as the observed diffusion coefficient measured using FCS matches what is expected for pure water (Fig. 1 *d*). Slower dynamics (increased viscosity) at the edges indicates a transition to a more gel-like state upon adding the complementary strand. Similar gelation upon basepairing was previously observed by Jain et al. (18) in DNA-spermine droplets. Furthermore, a preformed dsDNA immediately precipitates out of the solution upon mixing with PLL (Fig. 1 *e*) under the same conditions as in Fig. 1 *b*. This can be attributed to a higher charge density of dsDNA compared to ssDNA leading to stronger attractive interactions with PLL (19). Only under high salt (~830 mM NaCl) conditions, the dsDNA forms phase-separated liquid-like droplets (Fig. S4). Taken together, the results indicate that rigidity of dsDNA due to basepairing disfavors LLPS.

Role of local flexibility of ssDNA in LLPS

ssDNA and dsDNA have an order of magnitude difference between their respective persistence lengths (10–13,17). However, they also differ significantly in their linear charge densities, which could contribute to the observed differences in the phase behavior (20). Therefore, we employed 22-nt poly(A) and poly(T) ssDNA that have similar linear charge density. Although both poly(A) and poly(T) are often modeled as flexible polyelectrolytes, higher persistence lengths are reported for poly(A) (~7.8 nm for poly(A) versus 3.1 nm for poly(T)) (21), attributed to favorable stacking interactions between adjacent adenine bases (21–27). Furthermore, across a wide range of Na^+ concentrations, the magnitude of the scaling exponent for the radius of gyration, which is a measure of polymer chain flexibility, is higher for poly(A) compared to poly(T) (25). Based on these differences, we predicted poly(T) to undergo salt-dependent LLPS more readily. Both sequences form droplets over a wide range of salt concentrations (5–350 mM) (Fig. 2). However, at higher salt concentration (~500 mM), poly(A) shows very little phase separation. This observation correlates with differences in the flexibility, which is dominated by the intrinsic persistence length in the high salt regime. At ~1000 mM, no phase separation is observed because of complete charge screening. We also note that a 22-nt polycytidine (poly(C)), undergoes precipitation under conditions similar to Fig. 2. Droplets are formed only at mixing temperatures higher than the melting point of poly(C) (Figs. S5 and S6). This

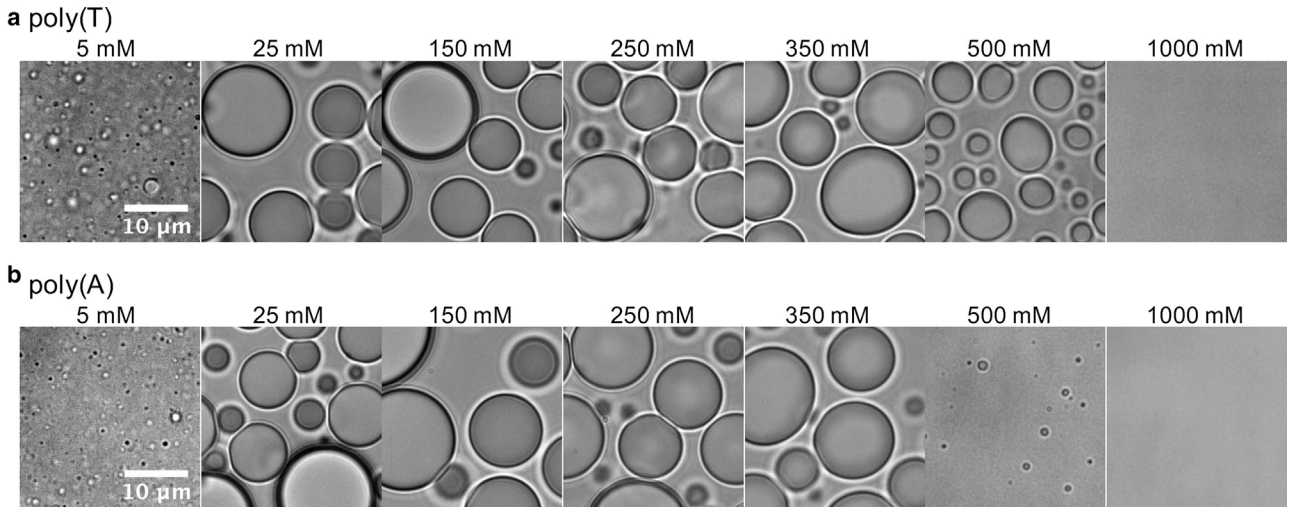

FIGURE 2 Local flexibility dependence of ssDNA LLPS in the presence of PLL. Bright-field microscopy images of (*a*) PLL-poly(T) and (*b*) PLL-poly(A) phases at different NaCl concentrations are shown; N/P ~1, room temperature. At 500 mM NaCl, poly(A) shows very little phase separation compared to poly(T), attributable to differences in intrinsic persistence lengths.

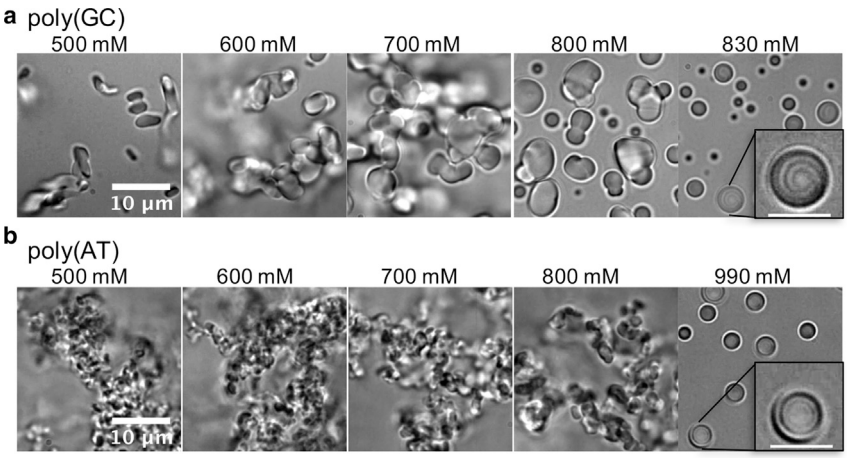

FIGURE 3 Local flexibility dependence of dsDNA LLPS in the presence of PLL. Bright-field microscopy images of (*a*) PLL-poly(GC) and (*b*) PLL-poly(AT) phases at different NaCl concentrations are shown; N/P ~1, room temperature. Poly(GC) forms droplets at much lower salt concentrations compared to poly(AT). At higher salt concentrations (830 mM for poly(GC) and 990 mM for poly(AT)), the LLPS gives rise to liquid-crystalline droplets. The striations observed in the droplets are characteristic of cholesteric phases. Inset scale bars, 5 μM.

is attributable to the presence of rigid basepaired structures (e.g., i-motifs) of poly(C) at room temperature (28,29).

Role of local flexibility of dsDNA in LLPS

The local flexibility of dsDNA is also dependent on its sequence (12,13,30). Although oligomers shorter than 150 bp are typically modeled as rigid rods, dsDNA is known to be locally flexible (30–32). It has been shown that AT-rich dsDNAs have higher intrinsic persistence lengths (~50.4 nm, estimated for AA/TT dinucleotide steps) compared to GC-rich dsDNAs (~41.7 nm, estimated for CC/GG dinucleotide steps) (30). Therefore, we designed palindromic poly(GC) and poly(AT) sequences to form dsDNA. Both sequences require much higher salt concentrations (>500 mM) compared to ssDNA to form droplets (Fig. 3), as predicted based on observations described in Fig. 1. However, compared to poly(AT), poly(GC) requires significantly less (~800 mM versus ~1000 mM) salt to form droplets, indicating that even a small difference in persistence length significantly impacts LLPS. There is a transition from precipitates at low salt concentrations to coarse droplets and then to spherical droplets (at 830 mM for poly(GC) and 990 mM for poly(AT)) as the salt concentration is increased. Interestingly, we find that the droplets formed at high salt concentrations are liquid-crystalline, as confirmed by polarized light microscopy (Fig. S7). Short dsDNA oligomers are known to from liquid-crystalline phases at high DNA concentrations via end-to-end stacking (33). In the PLL-dsDNA droplets, increased local DNA concentration is likely driven by polyelectrolyte complexation as PLL is also partitioned in the liquid-crystalline phase (Fig. S8). In addition, under a bright-field microscope, the striations observed in poly(GC) versus poly(AT) droplets differ, which could reflect ordering in the liquid-crystalline phase that depends on the physical properties of the DNA.

Role of free nucleotides in LLPS

Free nucleotides can promote LLPS by suppressing aggregation, which is the main process competing with LLPS. Perry et al. (34) observed chirality-selective LLPS in racemic mixtures of PLL that, in purely chiral mixtures, aggregated because of strong hydrogen bonding. Furthermore, ATP was recently shown to suppress protein aggregation by acting as a hydrotrope at millimolar concentrations (35). We therefore tested whether free NTPs promote droplet formation under the conditions of N/P and salt concentration at which dsDNA would otherwise precipitate. The composition was adjusted such that >50% of the total negative charges is replaced by NTP instead of dsDNA. At an N/P of ~1 and 150 mM salt, poly(GC) in the presence of ATP forms liquid-like droplets (Fig. 4 *a*; Fig. S9 *a*). YOYO-1-labeled poly(GC) is found to be partitioned inside the liquid-like droplets (Fig. S11). Under the same conditions, however, poly(AT) forms more gel-like droplets as evident from the bright-field and confocal images (Fig. 4 *b*; Fig. S9 *b*), demonstrating that dsDNA local flexibility also plays a role in LLPS in the presence of free nucleotides. The nucleotide UTP also promotes droplet formation (Figs. 5 and S12). However, higher concentrations of UTP were required to form droplets similar to PLL-dsDNA-ATP, indicating that LLPS is also dependent on the type of nucleotide.

Interestingly, we find that the PLL-dsDNA-NTP droplets tend to form liquid-crystalline subcompartments (as confirmed by polarized light microscopy; Figs. 4 and 5) that are different from the cholesteric phases observed in the absence of ATP (Fig. 2). All labeled components tend to partition less into these regions (Figs. S11–S13), possibly because of the tendency of fluorescent labels to disrupt the liquid-crystalline order. The formation of the subcompartments is likely due to two complexation processes (PLL with dsDNA and PLL with free ATP) occurring simultaneously such that the presence of ATP prevents large-scale precipitation of PLL-dsDNA, allowing for liquid-crystalline

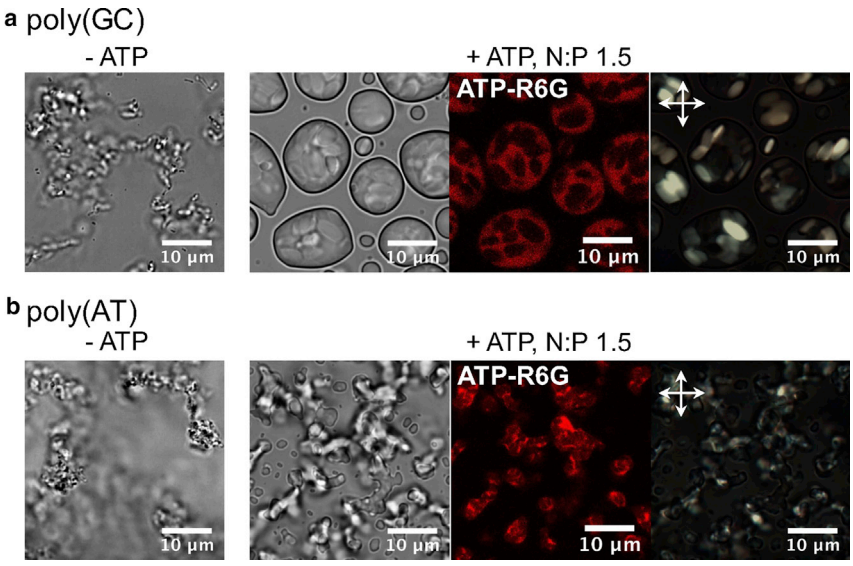

FIGURE 4 Role of ATP in LLPS of dsDNA. Bright-field and confocal microscopy images of (*a*) PLL-poly(GC) and (*b*) PLL-poly(AT) phases with and without ATP are shown. In the presence of ATP, liquid-like phases are formed; [NaCl] = 150 mM, N/P ~1 (ATP charge = 1.4 mM). The distribution of ATP inside the liquid-like phases is heterogeneous, giving rise to subcompartmented appearance. These subcompartments are dsDNA-rich liquid-crystalline phases, with the birefringent domains visible under cross-polarizers. Higher concentrations of ATP are required for poly(AT) compared to poly(GC) to form similar droplets (Fig. S10).

ordering inside a PLL-ATP liquid-like phase. From FCS data, fast transit times ($\tau_{transit}$ = 14 ms) of ATP-R6G partitioned in the brighter regions of PLL-poly(GC)-ATP droplets suggest liquid-like behavior. The transit times in the darker (liquid-crystalline) regions are significantly slower ($\tau_{transit}$ = 75 ms), as expected (Fig. S14 *a*). For ATP-R6G partitioned into PLL-poly(AT)-ATP droplets, the domains are not as well defined, and we are therefore unable to reliably make FCS measurements from brighter and darker regions exclusively (Fig. S14 *b*). In UTP-containing droplets, transit times of UTP-AF488 partitioned in the brighter regions are faster than transit times in darker regions (Fig. S15). Both timescales are faster than the transit times in the respective domains of ATP-containing droplets.

To test whether dsDNA remains basepaired in the NTP-containing droplets, we performed fluorescence cross correlation (FCCS) experiments using nanomolar amounts of a 22-bp dsDNA labeled at the 5′ ends of both complementary strands (poly(A)-ATTO647 and poly(T)-AF488) as the probe. FCCS measures the degree of crosscorrelation between two diffusing chromophores: strong crosscorrelation suggests coupled diffusion, whereas no correlation suggests independent diffusion. For preannealed dual-color poly(A-T), strong crosscorrelation is observed (Fig. S16 *a*), suggesting the DNA remains basepaired inside the droplets. No crosscorrelation is observed when labeled poly(A) and poly(T) are not preannealed, indicating that the two strands diffuse independently (Fig. S16 *b*).

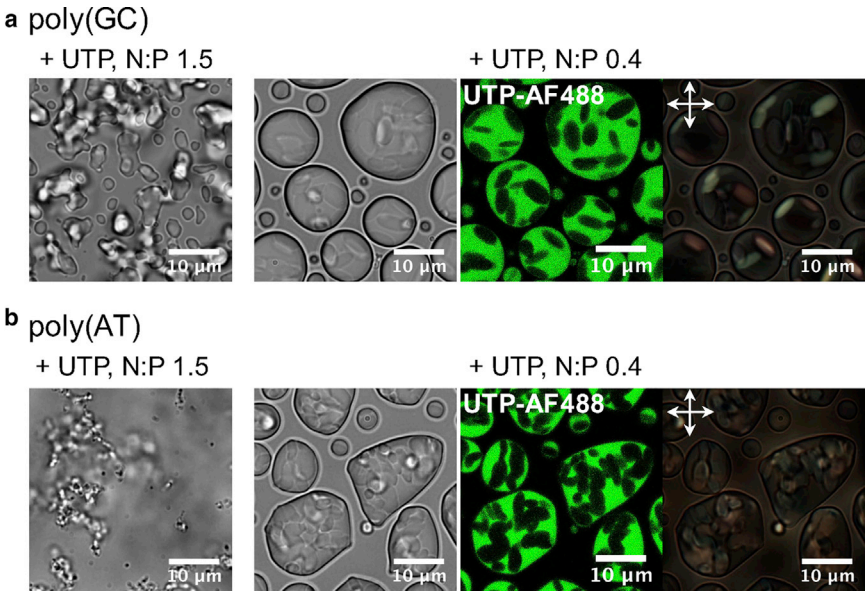

FIGURE 5 Role of UTP in LLPS of dsDNA. Bright-field and confocal microscopy images of (*a*) PLL-poly(GC) and (*b*) PLL-poly(AT) phases in the presence of UTP are shown; [NaCl] = 150 mM, N/P ~1 (UTP charge = 1.4 mM). The transition to liquid-like phases requires higher UTP concentration compared to ATP. At N/P ~0.2 (UTP charge = 7 mM), dsDNA-rich liquid-crystalline subcompartments are observed, with the birefringent domains visible under cross-polarizers.

CONCLUSIONS

Sequence-dependent LLPS has, to date, been considered an issue of charge patterning and correlation in either intrinsically disordered proteins (9,36,37) or synthetic polymers (37). In this study, we show that in polyelectrolytes with uniform charge distribution, the sequence can impart differences in local flexibility that contribute to LLPS. This extends to ternary systems (e.g. PLL-dsDNA-NTP) as well. Such dependence on local flexibility could provide a mechanism for selectivity in multicomponent LLPS. Within this context, it is interesting to note that GC-rich regions of genomic DNA are known to preferentially incorporate into nucleosomes, an effect attributed, at least in part, to the relative rigidity of AT tracts compared to GC tracts (38). Moreover, in light of recent studies on LLPS of heterochromatin proteins (5,6), local DNA flexibility could provide a new perspective to domain organization in the chromatin network.

In addition to membraneless intracellular organization, LLPS allows for reversible partitioning of molecules in liquid-like phases as well as responsiveness to environmental triggers (1,3,39). For example, some RNA-aggregation mediated diseases are thought to occur because of changes in the liquid-like state of membraneless organelles (18). Our observation that free NTPs promote LLPS of rigid DNA structures (Figs. 4 and 5) that otherwise precipitate under strong interaction conditions, could help understand regulation of LLPS in cells. Because both excessive intracellular LLPS and aggregation are generally undesirable, we envision entropy-based control (e.g., fluxional level of small molecules and flexible NA sequences) as a possible regulatory mechanism.

SUPPORTING MATERIAL

Sixteen figures are available at http://www.biophysj.org/biophysj/supplemental/S0006-3495(18)31103-2.

AUTHOR CONTRIBUTIONS

A.S. conceived and designed the project. A.S. and J.T.K. carried out experiments, analyzed data, and wrote the manuscript.

ACKNOWLEDGMENTS

We thank taxpayers who supported this work through the Korean Institute for Basic Science, project code IBS-R020-D1.

REFERENCES

1. Mitrea, D. M., and R. W. Kriwacki. 2016. Phase separation in biology; functional organization of a higher order. *Cell Commun. Signal.* 14:1–20.
2. Bergeron-Sandoval, L. P., N. Safaee, and S. W. Michnick. 2016. Mechanisms and consequences of macromolecular phase separation. *Cell.* 165:1067–1079.
3. Aguzzi, A., and M. Altmeyer. 2016. Phase separation: linking cellular compartmentalization to disease. *Trends Cell Biol.* 26:547–558.
4. Courchaine, E. M., A. Lu, and K. M. Neugebauer. 2016. Droplet organelles? *EMBO J.* 35:1603–1612.
5. Larson, A. G., D. Elnatan, …, G. J. Narlikar. 2017. Liquid droplet formation by HP1α suggests a role for phase separation in heterochromatin. *Nature.* 547:236–240.
6. Strom, A. R., A. V. Emelyanov, …, G. H. Karpen. 2017. Phase separation drives heterochromatin domain formation. *Nature.* 547:241–245.
7. Veis, A. 2011. A review of the early development of the thermodynamics of the complex coacervation phase separation. *Adv. Colloid Interface Sci.* 167:2–11.
8. Zhang, H., S. Elbaum-Garfinkle, …, A. S. Gladfelter. 2015. RNA controls PolyQ protein phase transitions. *Mol. Cell.* 60:220–230.
9. Lin, Y. H., J. D. Forman-Kay, and H. S. Chan. 2016. Sequence-specific polyampholyte phase separation in membraneless organelles. *Phys. Rev. Lett.* 117:178101.
10. Sim, A. Y. L. 2016. Nucleic acid polymeric properties and electrostatics: directly comparing theory and simulation with experiment. *Adv. Colloid Interface Sci.* 232:49–56.
11. Camunas-Soler, J., M. Ribezzi-Crivellari, and F. Ritort. 2016. Elastic properties of nucleic acids by single-molecule force spectroscopy. *Annu. Rev. Biophys.* 45:65–84.
12. Bao, L., X. Zhang, …, Z.-J. Tan. 2016. Flexibility of nucleic acids: from DNA to RNA. *Chin. Phys. B.* 25:018703.
13. Peters, J. P., III, and L. J. Maher. 2010. DNA curvature and flexibility in vitro and in vivo. *Q. Rev. Biophys.* 43:23–63.
14. Schneider, C. A., W. S. Rasband, and K. W. Eliceiri. 2012. NIH Image to ImageJ: 25 years of image analysis. *Nat. Methods.* 9:671–675.
15. Barrat, J. L., and J. F. Joanny. 1996. Theory of polyelectrolyte solutions. *Adv. Chem. Phys.* 94:1–66.
16. Dobrynin, A. V., and M. Rubinstein. 2005. Theory of polyelectrolytes in solutions and at surfaces. *Prog. Polym. Sci.* 30:1049–1118.
17. Smith, S. B., Y. Cui, and C. Bustamante. 1996. Overstretching B-DNA: the elastic response of individual double-stranded and single-stranded DNA molecules. *Science.* 271:795–799.
18. Jain, A., and R. D. Vale. 2017. RNA phase transitions in repeat expansion disorders. *Nature.* 546:243–247.
19. Bishop, K. J., C. E. Wilmer, …, B. A. Grzybowski. 2009. Nanoscale forces and their uses in self-assembly. *Small.* 5:1600–1630.
20. Vieregg, J. R., M. Lueckheide, …, M. V. Tirrell. 2018. Oligonucleotide-peptide complexes: phase control by hybridization. *J. Am. Chem. Soc.* 140:1632–1638.
21. Mills, J. B., E. Vacano, and P. J. Hagerman. 1999. Flexibility of single-stranded DNA: use of gapped duplex helices to determine the persistence lengths of poly(dT) and poly(dA). *J. Mol. Biol.* 285:245–257.
22. Goddard, N. L., G. Bonnet, …, A. Libchaber. 2000. Sequence dependent rigidity of single stranded DNA. *Phys. Rev. Lett.* 85:2400–2403.
23. Seol, Y., G. M. Skinner, …, A. Halperin. 2007. Stretching of homopolymeric RNA reveals single-stranded helices and base-stacking. *Phys. Rev. Lett.* 98:158103.
24. Ke, C., M. Humeniuk, …, P. E. Marszalek. 2007. Direct measurements of base stacking interactions in DNA by single-molecule atomic-force spectroscopy. *Phys. Rev. Lett.* 99:018302.
25. Sim, A. Y., J. Lipfert, …, S. Doniach. 2012. Salt dependence of the radius of gyration and flexibility of single-stranded DNA in solution probed by small-angle x-ray scattering. *Phys. Rev. E Stat. Nonlin. Soft Matter Phys.* 86:021901.
26. McIntosh, D. B., G. Duggan, …, O. A. Saleh. 2014. Sequence-dependent elasticity and electrostatics of single-stranded DNA: signatures of base-stacking. *Biophys. J.* 106:659–666.
27. Murphy, M. C., I. Rasnik, …, T. Ha. 2004. Probing single-stranded DNA conformational flexibility using fluorescence spectroscopy. *Biophys. J.* 86:2530–2537.

28. Gehring, K., J. L. Leroy, and M. Guéron. 1993. A tetrameric DNA structure with protonated cytosine.cytosine base pairs. *Nature.* 363:561–565.

29. Day, H. A., P. Pavlou, and Z. A. Waller. 2014. i-Motif DNA: structure, stability and targeting with ligands. *Bioorg. Med. Chem.* 22:4407–4418.

30. Geggier, S., and A. Vologodskii. 2010. Sequence dependence of DNA bending rigidity. *Proc. Natl. Acad. Sci. USA.* 107:15421–15426.

31. Vafabakhsh, R., and T. Ha. 2012. Extreme bendability of DNA less than 100 base pairs long revealed by single-molecule cyclization. *Science.* 337:1097–1101.

32. Mastroianni, A. J., D. A. Sivak, …, A. P. Alivisatos. 2009. Probing the conformational distributions of subpersistence length DNA. *Biophys. J.* 97:1408–1417.

33. Nakata, M., G. Zanchetta, …, N. A. Clark. 2007. End-to-end stacking and liquid crystal condensation of 6 to 20 base pair DNA duplexes. *Science.* 318:1276–1279.

34. Perry, S. L., L. Leon, …, M. Tirrell. 2015. Chirality-selected phase behaviour in ionic polypeptide complexes. *Nat. Commun.* 6:6052.

35. Patel, A., L. Malinovska, …, A. A. Hyman. 2017. ATP as a biological hydrotrope. *Science.* 356:753–756.

36. Pak, C. W., M. Kosno, …, M. K. Rosen. 2016. Sequence determinants of intracellular phase separation by complex coacervation of a disordered protein. *Mol. Cell.* 63:72–85.

37. Chang, L. W., T. K. Lytle, …, S. L. Perry. 2017. Sequence and entropy-based control of complex coacervates. *Nat. Commun.* 8:1273.

38. Torres, C. M., A. Biran, …, P. Scaffidi. 2016. The linker histone H1.0 generates epigenetic and functional intratumor heterogeneity. *Science.* 353:aaf1644.

39. Nott, T. J., E. Petsalaki, …, A. J. Baldwin. 2015. Phase transition of a disordered nuage protein generates environmentally responsive membraneless organelles. *Mol. Cell.* 57:936–947.